ROYAL SOCIETY OF CHEMISTRY

EDGE ARTICLE

Ternary hybrid CuO-PMA-Ag sub-1 nm nanosheet heterostructures†

Junli Liu,[a] Mingxin Wang,[a] Maria C. Dipalo,[a] Jing Zhuang,[a] Wenxiong Shi*[b] and Xun Wang [ID] *[a]

Multi-component two-dimensional (2D) hybrid sub-1 nm heterostructures could potentially possess many novel properties. Controlling the site-selective distribution of nanoparticles (NPs) at the edge of 2D hybrid nanomaterial substrates is desirable but it remains a great challenge. Herein, we realized for the first time the preparation of ternary hybrid CuO-phosphomolybdic acid-Ag sub-1 nm nanosheet heterostructures (CuO-PMA-Ag THSNHs), where the Ag NPs selectively distributed at the edge of 2D hybrid CuO-PMA sub-1 nm nanosheets (SNSs). And the obtained CuO-PMA-Ag THSNHs as the catalyst exhibited excellent catalytic activity in alkene epoxidation. Furthermore, molecular dynamics (MD) simulations demonstrated that the SNSs interact with Ag NPs to form stable nanoheterostructures. This work would pave the way for the synthesis and broader applications of multi-component 2D hybrid sub-1 nm heterostructures.

Introduction

Nanoheterostructures are usually defined as the combination of two nano-sized fragments into one entity,[1–3] which can be categorized as metal–metal,[4] metal–semiconductor[5,6] and semiconductor–semiconductor[7,8] according to the electronic structure of each unit. Benefiting from their complex structures and the wide range of applications in electronics,[9] optics,[10] catalysis,[11] *etc.* nanoheterostructures have drawn more and more attention in recent years.

Many synthetic strategies have been developed to prepare nanoheterostructures, mainly including wet-chemical and gas-phase methods.[1] The wet-chemical methods usually include heat-up or hot-injection in three-neck flasks[12–14] and hydro-thermal (solvothermal) methods,[15,16] most of which need to conduct complex growths and it is difficult to control the shape and size of products. Although the gaseous strategies (physical/chemical vapor deposition)[17–21] can realize the powerful control of the shape, size and composition of nanoheterostructures through the related parameter regulation, it is quite difficult to control the size of nanoheterostructures at the sub-1 nm scale. Atomic layer deposition (ALD) as an advanced atom-level vapor-phase deposition technique can create atomic-level epitaxial

growth, but it usually involves expensive apparatus and time-consuming operations.[22–24]

In our recent work, we proposed for the first time the 'cluster-nuclei co-assembly strategy' to realize controlling the component of materials at the sub-1 nm scale.[25] In this strategy, well-defined polyoxometalate (POM) clusters were introduced to intervene the nucleation of inorganic materials at the nucleation stage, where size-matched clusters interacted and co-assembled with inorganic nuclei to grow into different kinds of nanomaterials with sub-1 nm structures. Until now, we have successfully synthesized hybrid one-dimensional (1D) sub-1 nm nanobelt superstructures,[26] 2D sub-1 nm nanosheets,[27] 3D assemblies,[25] *etc.*, which exhibited highly efficient energy conversion, outstanding catalytic activity, *etc.*

Metal-oxide nanoheterostructures usually possess performances of metals and oxides leading to more research interest.[28] Although some metal-oxide nanoheterostructures have been reported, they usually only include two components. Meanwhile, how to control the size of metal-oxide nanoheterostructures at the sub-1 nm scale remains a great challenge. If the multi-component metal-oxide sub-1 nm nanoheterostructures could be prepared, due to the special sub-1 nm heterostructures and possible potential synergetic effect of multiple components, more excellent properties could be further explored.

Herein, we firstly synthesized ternary hybrid CuO-phosphomolybdic acid-Ag sub-1 nm nanosheet hetero-structures (CuO-PMA-Ag THSNHs). As shown in Scheme 1, 2D hybrid CuO-PMA sub-1 nm nanosheets (SNSs) were pre-synthesized by using the 'cluster-nuclei co-assembly strategy'. Firstly, PMA clusters were introduced to intervene the nucle-ation of CuO and they interacted and co-assembled into the CuO-PMA co-assembly. This as the building block continued to

[a]Key Lab of Organic Optoelectronics and Molecular Engineering, Department of Chemistry, Tsinghua University, Beijing 100084, China. E-mail: wangxun@mail.tsinghua.edu.cn

[b]Institute for New Energy Materials and Low Carbon Technologies, School of Materials Science and Engineering, Tianjin University of Technology, Tianjin 300387, China. E-mail: wxshi@email.tjut.edu.cn

† Electronic supplementary information (ESI) available. See DOI: 10.1039/d1sc02548a
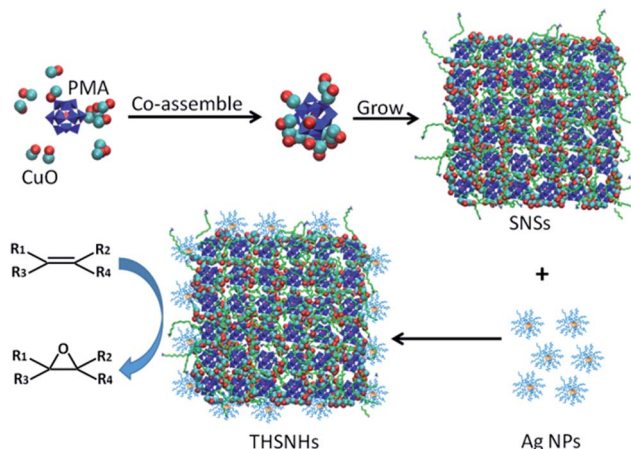
Scheme 1 Schematic illustration of the formation of CuO-PMA-Ag THSNHs. The red-blue models, blue models, orange-blue models, and green and blue link models represent the CuO molecules, PMA clusters, Ag NPs and oleylamine molecules, respectively.
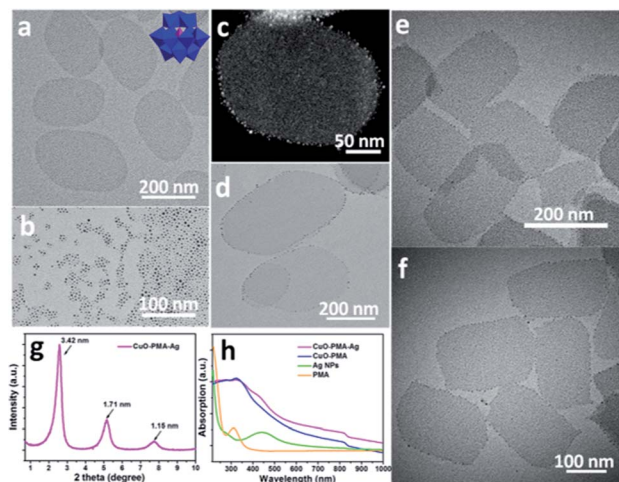

Fig. 1 Morphological images of the CuO-PMA-Ag THSNHs. (a) The TEM image of the CuO-PMA SNSs (the inset is the PMA molecule model). (b) The TEM image of Ag NPs. (c) The HAADF-STEM image of the CuO-PMA-Ag THSNHs. (d–f) The TEM images of CuO-PMA-Ag THSNHs. (g) The SAXRD pattern of the CuO-PMA-Ag THSNHs. (h) The UV-Vis spectra of PMA clusters, Ag NPs, CuO-PMA SNSs and CuO-PMA-Ag THSNHs.

grow into the CuO-PMA SNSs, in which the Ag nanoparticles (NPs) were deposited to obtain the CuO-PMA-Ag THSNHs. And this material as the catalyst showed excellent catalytic activity in alkene epoxidation due to the synergetic function of CuO-PMA SNSs and Ag NPs. Meanwhile, molecular dynamics (MD) simulations were performed to study the formation mechanism of the THSNHs and demonstrated that the CuO-PMA SNSs interact with Ag NPs to form stable nanoheterostructures, where the total potential energy of the system decreased during the process revealing that the system is energetically favorable.

Results and discussion

Preparation and characterization of the CuO-PMA-Ag THSNHs

Referring to our earlier work,[27] the CuO-PMA SNSs (Fig. 1a) were first synthesized by taking advantage of the 'cluster-nuclei co-assembly strategy'. Then a certain amount of pre-synthesized sub-1 nm Ag NPs (Fig. 1b) was added into the CuO-PMA SNS dispersion liquid to stir to obtain the CuO-PMA-Ag THSNHs. For details see the Experimental Section. Surprisingly, referring to the TEM images (Fig. 1d–f and S1†) and high angle annular dark field scanning transmission electron microscopy (HAADF-STEM) images (Fig. 1c and S2†) of the CuO-PMA-Ag THSNHs, we found that the Ag NPs only distributed along the edge of the CuO-PMA SNSs. Although when the CuO-PMA SNSs huddled, the Ag NPs still only existed at the edge of SNSs and no obvious Ag NPs could be observed in other places. And the distribution of Ag NPs in CuO-PMA-Ag THSNHs was specifically uniform. Furthermore, the small-angle X-ray diffraction (SAXRD) pattern of the THSNHs (Fig. 1g) suggested a typical layer structure. There appeared three peaks between 2° and 10°, which can be attributed to "00L" (L = 1, 2, 3). And according to Bragg's equation, the interlayer spacing was calculated to be 3.42 nm, which was rightly in agreement with the length of two alternating or bending oleylamine molecules. In addition, the X-ray diffraction (XRD) (Fig. S3†) and X-ray photoelectron spectroscopy (XPS) results (Fig. S4†) demonstrated that the CuO-PMA-Ag

THSNHs are made of copper oxide, molybdenum oxide and silver (0). In the XPS spectrum of Cu 2p (Fig. S4a†), two peaks of Cu $2p_{3/2}$ and Cu $2p_{1/2}$ appeared at 933.7 eV and 953.7 eV with splitting of 20 eV, which revealed the presence of Cu^{2+}. At the same time, the characteristic satellite peaks at 943.5 eV and 962.4 eV were in agreement with reported XPS data of CuO.[29–31] In the Mo 3d XPS spectrum (Fig. S4b†), the peaks at 232.2 and 235.2 eV can be attributed to Mo $3d_{5/2}$ and $3d_{3/2}$, respectively. It demonstrated the existence of molybdenum oxides.[32,33] In the Ag XPS spectrum (Fig. S4c†), the peaks at 368.2 and 374.2 eV corresponded to Ag $3d_{5/2}$ and $3d_{3/2}$, respectively, which suggested that the valence of Ag is 0.[34,35] Moreover, the ultraviolet-visible (UV-Vis) spectra of CuO-PMA-Ag THSNHs, CuO-PMA SNSs, PMA and Ag NPs (Fig. 1h) revealed that the PMA clusters and Ag NPs are really present in the CuO-PMA-Ag THSNHs. Furthermore, the Fourier-transform infrared (FT-IR) spectra (Fig. S5†) and electrospray ionization ion trap-time of flight (ESI IT-TOF) spectrum of CuO-PMA-Ag THSNHs (Fig. S6†) also directly demonstrated the existence of PMA clusters in the final products. And the corresponding chemical formula of the THSNHs was given as $(CuO)_{0.2489}(PMo_{12}O_{40})Ag_{0.009290}$ according to the inductively coupled plasma optical emission spectroscopy (ICP-OES) data (Table S1†). In addition, this method to synthesize multi-component hybrid sub-1 nm heterostructures could also be extended to other kinds of THSNHs. As shown in Fig. S7,† the CuO-PMA-PtP THSNHs were obtained by using the same strategy, which demonstrated the generality of this method.

Molecular dynamics (MD) simulations

The 'cluster-nuclei co-assembly strategy' was proposed for the first time in our earlier work, where the clusters interacted and co-assembled with inorganic nuclei at the nucleation stage and

grew into nanomaterials with sub-1 nm architectures.[25] So on the basis of this mechanism, the 2D hybrid CuO-PMA SNSs with uniform shape and size were synthesized.[27] And in that work, MD simulations were used to investigate the formation mechanism. It demonstrated that protonated oleylamine molecules (OLY) were used to neutralize the total charge of the system and CuO molecules interacted with PMA clusters to co-assemble into 2D simple square SNSs, which can remain stable.

In this work, we firstly prepared the 2D hybrid CuO-PMA SNSs according to the earlier work,[27] and on the basis of MD simulations of the CuO-PMA SNSs, we continued to try to study the interaction between Ag NPs and CuO-PMA SNSs in the CuO-PMA-Ag THSNHs. Firstly, in order to investigate the reaction between Ag NPs and CuO-PMA SNSs, 16 Ag NPs capped by oleylamine (OLL) were placed in the surrounding of 25.2 nm × 24.5 nm CuO-PMA SNSs as shown in Fig. 2a and b, the ratios of which
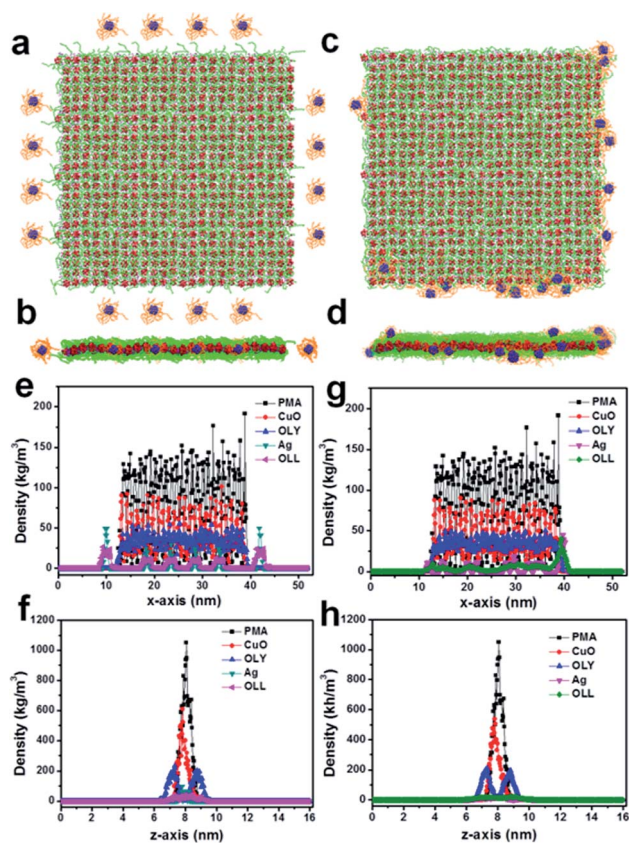

Fig. 2 MD simulations of the CuO-PMA-Ag THSNHs. (a) The top view and (b) the side view of the initial model when 16 Ag NPs were placed in the surroundings of 25.2 nm × 24.5 nm CuO-PMA SNSs. (c) The top view and (d) the side view of the CuO-PMA-Ag THSNH model after running the simulation. The continuous density distributions of PMA, CuO, OLY, Ag and OLL in the initial model along the (e) x-axis and (f) z-axis. The continuous density distributions of PMA, CuO, OLY, Ag and OLL in the CuO-PMA-Ag THSNH model after running the simulation along the (g) x-axis and (h) z-axis (The red models represent PMA clusters. The small blue-purple models stand for CuO molecules. The green chain models represent the oleylamine molecules in the CuO-PMA SNSs, which were annotated as OLY. The blue models stand for Ag NPs. The orange chain models represent the oleylamine molecules on the surface of Ag NPs, which were annotated as OLL).

were obtained according to the ICP-OES results (Table S1†). Fig. 2e and f displayed the density distributions of PMA, CuO, OLY, Ag and OLL in THSNHs along the x-axis and z-axis at the start of simulations, which were corresponding to Fig. 2a and b (in order to distinguish the oleylamine molecules located on the CuO-PMA SNSs and Ag NPs, the green chain models were used to represent the oleylamine molecules on the CuO-PMA SNSs, which were annotated as OLY and the orange chain models represented the oleylamine molecules on the surface of Ag NPs, which were annotated as OLL. In the following energy part, we would study the effect of OLL on system energy). Movie S1† showed the dynamic simulation process. At the beginning, Ag NPs moved randomly, where only the position of PMA was frozen. And with the time prolonging, the Ag NPs gradually fixed at the edge of CuO-PMA SNSs to form the THSNHs after running the simulation (Fig. 2c and d), and the density distribution was shown in Fig. 2g and h. By analyzing the density distributions of multiple components before and after simulation, we found that the distance between Ag NPs reduced and others almost not changed during the simulation process. Meanwhile, the MD simulation results revealed that although the Ag NPs move randomly, they preferred to stay at the edge of SNSs at the end. And once the Ag NPs touched the SNSs, they would not leave. All of these suggested that the CuO-PMA-Ag THSNHs possess a quite stable structure. In addition, the thin edge size of the CuO-PMA sub-1 nm nanosheets led to the lower surfactant adsorption. So the edge belongs to the weak area for surfactants, and silver nanoparticles may break through the protection of surfactants and adsorbed at the edge of CuO-PMA easily. However, the surface area of nanosheets was large, and the multi-surfactant stretching activity had a high probability of pushing away silver, which led to the unique site-selective distribution of silver nanoparticles.

Moreover, in order to further explore the stability of the THSNHs, we also studied the CuO-PMA-Ag THSNHs from the energy point of view. The interaction energy between one Ag NP and CuO-PMA SNS was taken as the research object to be investigated. The results suggested that the interaction energy (including Lennard-Jones (LJ) potential energy, Coulomb energy, etc.) between the CuO-PMA SNS and OLL was the main driving force for the formation of CuO-PMA-Ag THSNHs (Fig. 3a). And the LJ potential energy between the SNS and Ag atoms played a role after the Ag NPs touched the CuO-PMA SNS as shown in Fig. 3b, which worked after the interaction energy between OLL and SNS. On the basis of above investigation, the total interaction energy (including SNS-OLL and SNS-Ag) was also given in Fig. 3c. Meanwhile, we found that the total potential energy of the system decreased during the simulation process according to Fig. 3d, which revealed that the system is energetically favorable. And it also further proved that the Ag NPs interact with the CuO-PMA SNSs to assemble into the stable CuO-PMA-Ag THSNHs.

Catalytic performances of the CuO-PMA-Ag THSNHs in alkene epoxidation

Alkene epoxidation is a vital reaction in the fine chemical industry. And the resultant epoxides are important
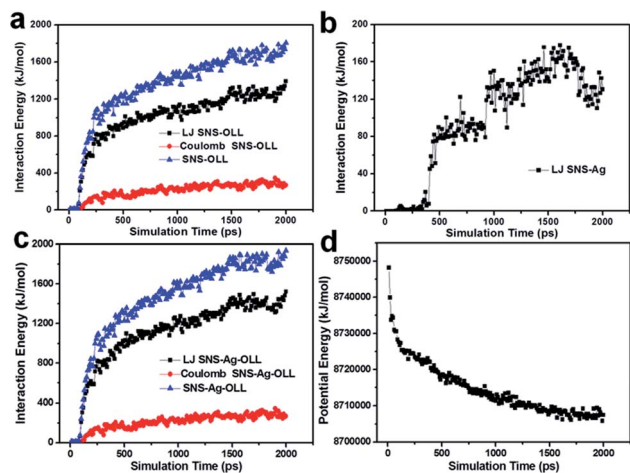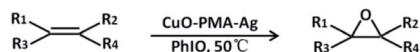
Fig. 3 Interaction energy of the CuO-PMA-Ag THSNHs. (a) The evolution of total interaction energy (blue curve), LJ potential energy (black curve) and Coulomb energy (red curve) between the SNS and OLL in one Ag NP. (b) The evolution of LJ potential energy between the SNS and bare Ag atoms in one Ag NP. (c) The evolution of total interaction energy (blue curve), LJ potential energy (black curve) and Coulomb energy (red curve) between one Ag-OLL NP and the SNS. (d) The potential energy of the whole system.
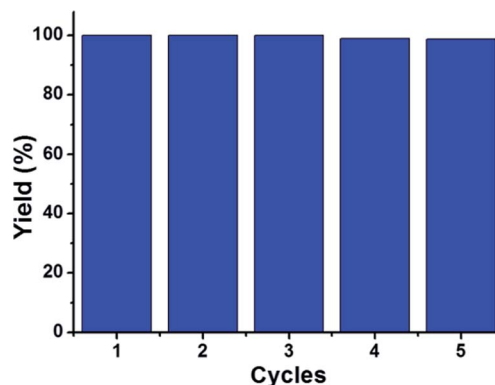

Fig. 4 Stability studies. The catalytic experiments were carried out by using the recycled CuO-PMA-Ag THSNH catalyst for the epoxidation of cyclohexene under the same reaction conditions.

intermediates in the preparation of plasticizers, cosmetics, epoxide resins, medicines, *etc.* According to some reported studies, copper oxide-based[36,37] and silver-based nanomaterials[38] have shown active catalytic activity in the epoxidation of alkenes. However, these reactions usually need to be performed at high temperature or consume more time.[39,40] Inspired by these, considering the obtained CuO-PMA-Ag THSNHs as the combination of copper oxide and silver, we tried to apply this material as the catalyst to the epoxidation of alkenes, where iodosobenzene (PhIO) and chloroform (CHCl$_3$) were used as the oxidant and solvent, respectively, and the reaction happened at 50 °C. As shown in Table 1, the CuO-PMA-Ag THSNH catalyst showed excellent catalytic activity in the epoxidation of alkenes (including cyclohexene, 1-octene and *cis*-stilbene). At 50 °C, the catalytic epoxidation of *cis*-stilbene can reach a conversion of 99.34% within 4 hours. And a higher conversion of 100% was achieved when the substrate was 1-

octene within 3 hours under the same reaction conditions. Especially, in the epoxidation reaction of cyclohexene, the conversion reached up to 100% just in 2 hours, which consumed less time than the other two reactions. This can be attributed to the steric hindrance of carbon chains and aryl–aryl in alkenes. At the same time, control experiments were performed under the same conditions for the same or longer reaction time as above by using single CuO-PMA SNS and sub-1 nm Ag NP catalysts, the results of which were displayed in Table S2.† We found that even when the reaction time was prolonged, both CuO-PMA SNS and Ag NP catalysts showed worse catalytic activity, and the reaction rate and conversion were obviously lower than those of the CuO-PMA-Ag THSNH catalyst. This revealed that the THSNHs are really the ideal catalyst for the olefin epoxidation reaction, and it can be attributed to the synergetic effect of multiple components. Meanwhile, the special nanoheterostructures also played an important role in this reaction. On the one hand, the special 2D sub-1 nm nanosheets with larger area could provide more active sites, and on the other hand, the combination of CuO-PMA and Ag produced a new interface, which also may produce new active sites. All of the above factors led to more efficient catalytic activity than previous studies for the alkene epoxidation. As shown in Table S3,† some reported materials used to catalyze the alkene epoxidation were listed. Moreover, stability is also a vital factor to evaluate the performance of catalysts. In Fig. 4, the recycling stability of the CuO-PMA-Ag THSNH catalyst was investigated, where cyclohexene was the substrate. Obviously, after five cycles, the conversion of the epoxides still remained nearly 100%, which demonstrated that the CuO-PMA-Ag THSNH catalyst really possesses excellent stability.

Conclusions

In conclusion, we successfully prepared CuO-PMA-Ag THSNHs by depositing Ag NPs in 2D CuO-PMA SNSs, where the Ag NPs distributed uniformly at the edge of CuO-PMA SNSs. MD simulations demonstrated that CuO-PMA SNSs interact with Ag NPs to form stable nanoheterostructures, where the total potential energy of the system decreased during the process

Table 1 Catalytic performance of the CuO-PMA-Ag THSNH catalyst in the epoxidation of alkenes. Conditions: 12 mg of CuO-PMA-Ag THSNH catalyst was dispersed into 1 ml of CHCl$_3$, and 60 mg of PhIO and 3 µl of alkenes were added and stirred at 50 °C. GC-MS measurements were performed to obtain the conversion

Entry	Alkene	Time (h)	Conversion (%)
1	Cyclohexene	2	100
2	1-Octane	3	100
3	*Cis*-stilbene	4	99.34

revealing that the system is energetically favorable. Meanwhile, the obtained THSNHs as the catalyst showed excellent catalytic activity in the epoxidation of alkenes, which can be attributed to the synergetic effect of multiple components and the special sub-1 nm nanoheterostructures providing more active sites. We believe our work would pave the way for the preparation of multi-component 2D hybrid sub-1 nm heterostructures with more novel properties for a wider range of applications.

Author contributions

X. W. led the project. J. L. designed, carried out the experiments, analyzed data about the CuO-PMA-Ag THSNHs and wrote the paper. S. W. performed molecular dynamics simulations. M. W., M. D. and J. Z. provided professional suggestion.

Conflicts of interest

There are no conflicts to declare.

Acknowledgements

Notes and references

1 B. Xu, G. Zhou and X. Wang, *NPG Asia Mater.*, 2015, **7**, e164.
2 P. D. Cozzoli, T. Pellegrino and L. Manna, *Chem. Soc. Rev.*, 2006, **35**, 1195–1208.
3 R. Costi, A. E. Saunders and U. Banin, *Angew. Chem.*, 2010, **49**, 4878–4897.
4 T. Pellegrino, A. Fiore, E. Carlino, C. Giannini, P. D. Cozzoli, G. Ciccarella, M. Respaud, L. Palmirotta, R. Cingolani and L. Manna, *J. Am. Chem. Soc.*, 2006, **128**, 6690–6698.
5 C. Pacholski, A. Kornowski and H. Weller, *Angew. Chem.*, 2004, **43**, 4774–4777.
6 T. Mokari, E. Rothenberg, I. Popov, R. Costi and U. Banin, *Science*, 2004, **304**, 1787–1790.
7 S. K. Han, M. Gong, H. B. Yao, Z. M. Wang and S. H. Yu, *Angew. Chem.*, 2012, **51**, 6365–6368.
8 T. T. Zhuang, F. J. Fan, M. Gong and S. H. Yu, *Chem. Commun.*, 2012, **48**, 9762–9764.
9 J. S. Lee, E. V. Shevchenko and D. V. Talapin, *J. Am. Chem. Soc.*, 2008, **130**, 9673–9675.
10 J. Zhang, Y. Tang, K. Lee and M. Ouyang, *Nature*, 2010, **466**, 91–95.
11 J. Yang and J. Y. Ying, *Angew. Chem.*, 2011, **50**, 4637–4643.
12 Y. W. Jun, J. S. Choi and J. Cheon, *Angew. Chem.*, 2006, **45**, 3414–3439.
13 L. Carbone and P. D. Cozzoli, *Nano Today*, 2010, **5**, 449–493.

14 J. Park, J. Joo, S. G. Kwon, Y. Jang and T. Hyeon, *Angew. Chem.*, 2007, **46**, 4630–4660.
15 T. I. Lee, S. H. Lee, Y. D. Kim, W. S. Jang, J. Y. Oh, H. K. Baik, C. Stampfl, A. Soon and J. M. Myoung, *Nano Lett.*, 2012, **12**, 68–76.
16 B. Xu, P. He, H. Liu, P. Wang, G. Zhou and X. Wang, *Angew. Chem.*, 2014, **53**, 2339–2343.
17 C. Li, Y. Yu, M. Chi and L. Cao, *Nano Lett.*, 2013, **13**, 948–953.
18 M. J. Bierman, Y. K. Lau, A. V. Kvit, A. L. Schmitt and S. Jin, *Science*, 2008, **320**, 1060–1063.
19 Y. J. Hwang, C. H. Wu, C. Hahn, H. E. Jeong and P. Yang, *Nano Lett.*, 2012, **12**, 1678–1682.
20 M. Chen, A. Zhang, Y. Liu, D. Cui, Z. Li, Y.-H. Chung, S. P. Mutyala, M. Mecklenburg, X. Nie, C. Xu, F. Wu, Q. Liu and C. Zhou, *Nano Res.*, 2020, **13**, 2625–2631.
21 J. Lin, H. Wang, R. Y. Tay, H. Li, M. Shakerzadeh, S. H. Tsang, Z. Liu and E. H. T. Teo, *Nano Res.*, 2020, **13**, 2371–2377.
22 S. M. George, *Chem. Rev.*, 2010, **110**, 111–131.
23 J. Xie, X. Yang, B. Han, Y. Shao-Horn and D. Wang, *ACS Nano*, 2013, **7**, 6337–6345.
24 Y. Huang and L. Liu, *Sci. China Mater.*, 2019, **62**, 913–924.
25 J. Liu, W. Shi, B. Ni, Y. Yang, S. Li, J. Zhuang and X. Wang, *Nat. Chem.*, 2019, **11**, 839–845.
26 J. Liu, N. Liu, H. Wang, W. Shi, J. Zhuang and X. Wang, *J. Am. Chem. Soc.*, 2020, **142**, 17557–17563.
27 J. Liu, W. Shi and X. Wang, *J. Am. Chem. Soc.*, 2019, **141**, 18754–18758.
28 L. Li, X. Chen, Y. Wu, D. Wang, Q. Peng, G. Zhou and Y. Li, *Angew. Chem.*, 2013, **52**, 11049–11053.
29 W. Yao, Y. Zhang, T. Duan, W. Zhu, Z. Yi and X. Cui, *Phys. B*, 2016, **493**, 7–13.
30 C. Song, Z. Zhao, H. Li, D. Wang and Y. Yang, *RSC Adv.*, 2016, **6**, 102931–102937.
31 Z. Guo, M. L. Seol, M. S. Kim, J. H. Ahn, Y. K. Choi, J. H. Liu and X. J. Huang, *Nanoscale*, 2012, **4**, 7525–7531.
32 A. M. Dejong, H. J. Borg, L. J. Vanijzendoorn, V. G. F. M. Soudant, V. H. J. Debeer, J. A. R. Vanveen and J. W. Niemantsverdriet, *J. Phys. Chem. C*, 1993, **97**, 6477–6483.
33 M. Anwar, C. A. Hogarth and R. Bulpett, *J. Mater. Sci.*, 1990, **25**, 1784–1788.
34 Y. Liu, R. G. Jordan and S. L. Qiu, *Phys. Rev. B: Condens. Matter Mater. Phys.*, 1994, **49**, 4478.
35 R. B. Shalvoy, G. B. Fisher and P. J. Stiles, *Phys. Rev. B: Condens. Matter Mater. Phys.*, 1977, **15**, 1680.
36 N. Scotti, N. Ravasio, F. Zaccheria, R. Psaro and C. Evangelisti, *Chem. Commun.*, 2013, **49**, 1957–1959.
37 C. Chen, J. Qu, C. Cao, F. Niu and W. Song, *J. Mater. Chem.*, 2011, **21**, 5774–5779.
38 P. Christopher and S. Linic, *J. Am. Chem. Soc.*, 2008, **130**, 11264.
39 Z. Ye, L. Hu, J. Jiang, J. Tang, X. Cao and H. Gu, *Catal. Sci. Technol.*, 2012, **2**, 1146–1149.
40 L. Hu, L. Shi, H. Hong, M. Li, Q. Bao, J. Tang, J. Ge, J. Lu, X. Cao and H. Gu, *Chem. Commun.*, 2010, **46**, 8591–8593.